

Physico-Chemical Properties of New Liquid Crystals Incorporating a Benzofuran-2-one Skeleton

Yuki Morita, Fusheng Zhang, Takeyasu Tasaka, Remuto Yamaguchi, Hiroaki Okamoto, and Shunsuke Takenaka*

Department of Advanced Materials and Science, Faculty of Engineering, Yamaguchi University, 2-16-1 Tokiwadai, Ube 755-8611

Received August 5, 2005; E-mail: takenaka@po.cc.yamaguchi-u.ac.jp

The liquid crystal properties of 3*H*-2-oxobenzofuran-6-yl 4-(*n*-$C_nH_{2n+1}O$)benzoates (**1**-*n*, $n = 5$–12), 4′-(*n*-$C_nH_{2n+1}O$)biphenyl-4-carboxylates (**2**-*n*, $n = 6$–10), and 4-(*n*-C_nH_{2n+1})benzoates (**3**-*n*, $n = 4$–6) are described. The $n = 5$–8 homologues of **1**-*n* exhibit a nematic (N) phase, and the $n = 8$–12 homologues exhibit a smectic A (SmA) phase, where the layer spacing is ca. 1.3 times of the calculated molecular length. The homologues of **2**-*n* show a complex phase-transition behavior involving a smectic C (SmC), two kinds of SmA, reentrant nematic, and N phases, where the SmC phase is exhibited by the $n = 6$–8 homologues. The layer spacings of SmA phases formed at high and low temperature regions correspond to 1.3 and 1.0 times of the molecular lengths, respectively. The polar interactions around the terminal lactone moiety are assumed to play important roles for the complex polymesomorphism and diversity of the smectic layer structure.

It is well known that terminal polar groups such as benzonitriles or nitrobenzenes play important roles in determining physical properties of liquid crystal (LC) molecules. Especially, polar interactions such as dipole–dipole and dipole-induced dipole have been considered to result in various complex polymesomorphisms involving some smectic A (SmA) and C (SmC) phases and a reentrant nematic (N_{re}) phase and diversity of the smectic layer structure.[1] Although benzonitrile or the nitrobenzene is certainly apt to consider as typical examples of polar functional group, some lactone compounds also possess a large dipole moment, as shown in Fig. 1. In Fig. 1, μ_{obs} and μ_{cal} indicate the observed and calculated (MOPAC2000(AM1)) dipole moments, respectively. A carbonyl group intrinsically has a large dipole moment, namely D = 2.29 for formaldehyde,[2] so that materials incorporating the carbonyl group at the terminal position exhibit a "polar" SmA phase.[3] Furthermore, ester compounds are intrinsically expected to have a much larger dipole moment than the carbonyl compounds due to an electronic distortion on two oxygen atoms. In practice, however, the observed dipole moments of many esters are not so large. For example, the dipole moment is 1.78 D for ethyl acetate.[4] Cancellation of the electronic distortion in the most stable zigzag conformation shown in Fig. 1 should be responsible for the reduction. The reduction of the dipole moments for ethyl acetate is also suggested from the result of a semi-empirical molecular orbital calculation (MOPAC2000), as shown in Fig. 1. In contrast, cyclic esters (lactones), such as furan-2(5*H*)-one ($\mu_{obs} = 4.62$ D)[5] and 5,6-dihydropyran-2-one ($\mu_{obs} = 5.08$ D),[6] have much larger dipole moments than the esters, since the cancellation of the electronic distortion should not occur in their cyclic structures. The dipole moments of lactone compounds also compare with those of benzonitrile and nitro-

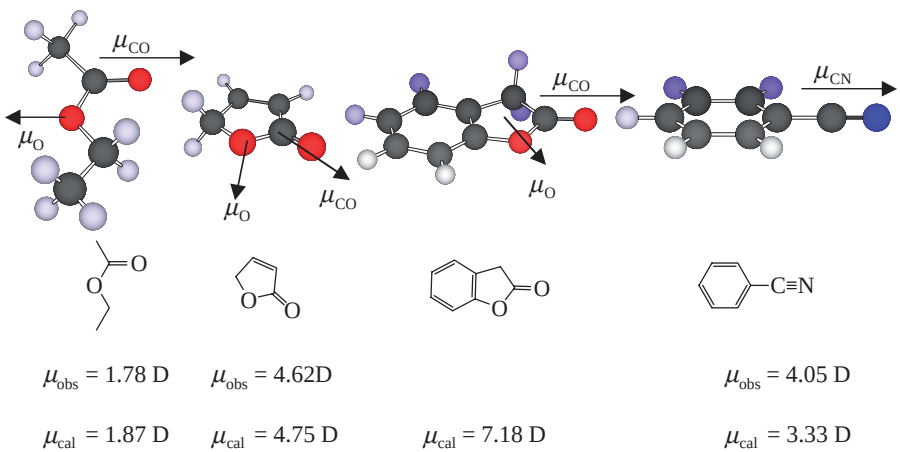

Fig. 1. Molecular structures and observed (μ_{obs}) and calculated (μ_{cal}) dipole moments (D). Dipole moments (μ_{cal}) were calculated by MOPAC2000, where the heat of formation was minimized by an AM1 method.

Published on the web January 13, 2006; DOI 10.1246/bcsj.79.163

benzene.[7] Interestingly, the MO calculation predicts that 3*H*-benzofuran-2-one has a large dipole moment ($\mu_{cal} = 4.18$ D) and keeps a planar structure, so that the core is quite attractive for a component of LC materials. Of course, the practical molecular dipole moment is not always proportional to the magnitude calculated by MOPAC2000.

This work aims at the development of new LC materials incorporating a 3*H*-benzofuran-2-one skeleton and explication of the electrostatic effect of the lactone skeleton on the physico-chemical properties. For this purpose, we designed and prepared new LC materials **1**-*n*–**3**-*n*, whose structures are shown in Fig. 2. The MO calculation predicts that the carbonyl axis of the benzofuran-2-one skeleton declines a little to the average axis of the aromatic moiety and that a part of the skeleton protrudes from the rod of the LC core.

The formation of smectic phases and the layer structure are discussed in terms of the molecular properties predicted by the MO calculation.

Results and Discussion

Thermal Properties. Phase-transition behavior for **1**-*n*–**3**-*n* is summarized in Tables 1–3, respectively. The pentyloxy–octyloxy homologues of **1**-*n* exhibit a monotropic N phase, and the N–I transition temperature gradually rises with increasing *n*. The N–I transition temperatures show a weak even–odd alternation in the range between the pentyloxy and octyloxy homologues. An enantiotropic SmA phase is also exhibited by the nonyloxy–dodecyloxy homologues, where the SmA–I transition temperature gradually rises with increasing *n*. A similar tendency is also observed in polar LC materials with a small LC core, such as 4-alkoxyphenyl 4-cyanobenzoates and 4-cyanophenyl 4-alkoxybenzoates.[8,9]

Transition temperatures are plotted against *n* in Fig. 3. The homologues of **2**-*n* show a complex polymesomorphism. A monotropic SmA phase, namely the SmA (1) phase in Table 2, is exhibited by the pentyloxy and hexyloxy homologues, where the SmA (1)–N transition temperature tends to fall with increasing *n*. A monotropic SmC phase is exhibited by the hexyloxy, heptyloxy, and octyloxy homologues, where the SmC–SmA (1) or SmC–N transition temperature also falls with increasing *n*. As shown in Table 2, the latent heats for the SmC–SmA (N) transition were so small that the phase transition could be

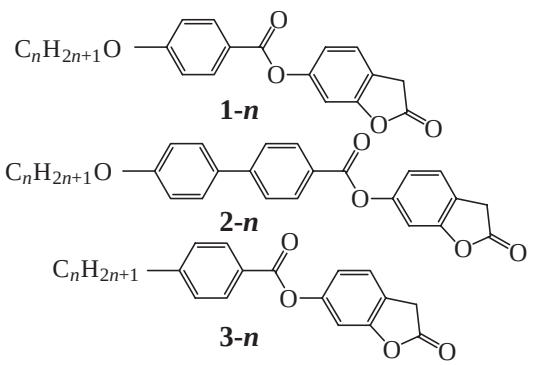

Fig. 2. Molecular structures of **1**-*n*–**3**-*n*.

Table 1. Transition Temperatures and Latent Heats of **1**-*n*[a)]

n	C		SmA		N		I
5	•	81	—		(•	35)	•
		28.5				—[b)]	
6	•	63	—		(•	50)	•
		31.3				0.4	
7	•	72	—		(•	53)	•
		29.7				0.4	
8	•	75	(•	58	•	62)	•
		22.1		—[b)]		0.8	
9	•	56	•	72	—		•
		21.7		1.4			
10	•	58	•	81	—		•
		23.5		1.9			
11	•	60	•	86	—		•
		25.9		2.4			
12	•	65	•	89	—		•
		31.3		3.0			

a) Upper and lower columns indicate transition temperatures (°C) and latent heats (kJ mol^{-1}), respectively. Parentheses indicate a monotropic transition. C, SmA, N, and I indicate crystal, smectic A, nematic, and isotropic phases, respectively. b) The separate peak due to the N–SmA transition could not be obtained due to rapid recrystallization.

Table 2. Transition Temperatures and Latent Heats of **2**-*n*[a)]

n	C		SmC		SmA (1)		N_{re}		SmA (2)		N		I
5	•	143	—		(•	127)	—		—		•	222	•
		27.1				0.9						0.5	
6	•	114	(•	101	•	113)	—		—		•	218	•
		26.6		0		0.5						0.4	
7	•	113	(•	93)	—		—		—		•	211	•
		30.1		0								0.5	
8	•	109	(•	83	—		•	105)	•	185	•	207	•
		21.6		0				0		0.1		0.6	
9	•	106	—		—		—		•	200	•	205	•
		28.6								3.1			
10	•	104	—		—		—		•	206	—		•
		25.6								2.1			

a) Upper and lower columns indicate transition temperatures (°C) and latent heats (kJ mol^{-1}), respectively. Parentheses indicate a monotropic transition. SmC, N_{re}, and SmA (1 and 2) indicate smectic C, reentrant nematic, and two different kinds of smectic A phases, respectively.

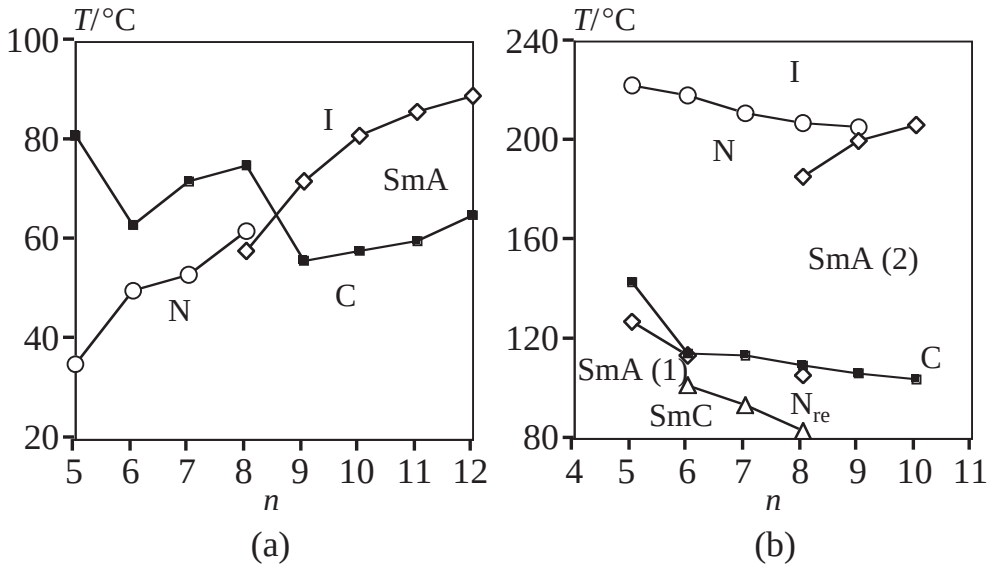

Fig. 3. Plots of transition temperatures vs *n* for: (a) **1**-*n* and (b) **2**-*n*. Phase transitions below melting points were observed on the monotropic process.

Table 3. Transition Temperatures of **3**-*n* (°C)

n	C		I
4	•	53	•
5	•	68	•
6	•	63	•

detected only by microscopic observation. The SmA (1) and SmC phases were characterized by microscopic observation and the results are shown in Fig. 4. The micrographic texture of the SmA (1) phase fundamentally consists of a fine focal-conic fan or a marble organization under a homogeneous alignment and a dark sheer alignment under a homeotropic one, as shown in Fig. 4a. On the other hand, the micrograph texture of the SmC phase has a schlierene organization under the homeotropic alignment, as shown in Fig. 4b, though the texture is quite similar to that of the SmA (1) phase under the homogeneous alignment. These results indicate that the SmA (1) and SmC phases classified in this section possess optically uni- and bi-axial natures, respectively.

The octyloxy homologue shows another kind of SmA phase, namely SmA (2), where the SmA (2)–N transition temperature is very high and the new N phase N_{re} is exhibited below the SmA (2) phase, as well as the SmC phase at the monotropic region. The micrographic texture and optical properties of the SmA (2) phase are similar to those of the SmA (1) phase. The latent heats of the SmC–N_{re} and N_{re}–SmA (2) transitions were too small to be numerated by DSC. Therefore, the SmC–N_{re} and N_{re}–SmA (2) transition temperatures in Table 2 were determined only by microscopic observation.

The nonyloxy homologue shows SmA and N phases, and the N_{re} phase could be observed neither by DSC nor microscopic observation. The SmA–N transition temperature is close to that of **2**-8, so that the SmA phase should have similar physical properties to those of the SmA (2) phase exhibited by the octyloxy homologue. The phase-transition behavior is illustrated in Fig. 3b.

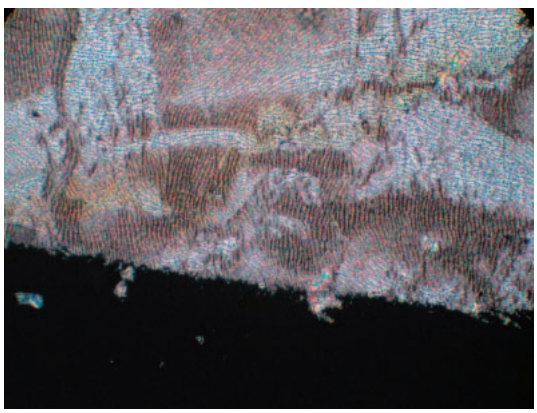

(a)

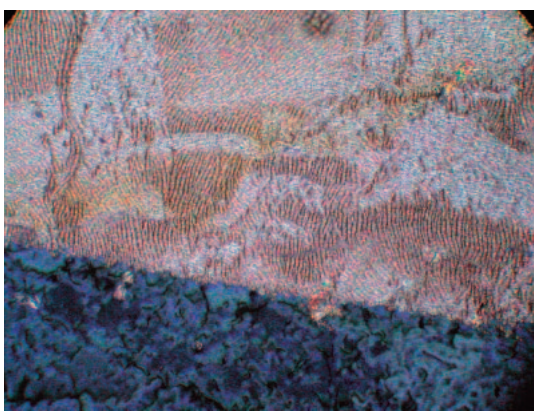

(b)

Fig. 4. Micrographs of: (a) SmA (1) at 110 °C and (b) SmC phases at 96 °C for **2**-6.

The alkyl compounds **3**-*n* do not exhibit any mesophase, even in a rapid cooling process, indicating that the terminal alkyl group does not give LC properties in the 2-oxobenzofuran-

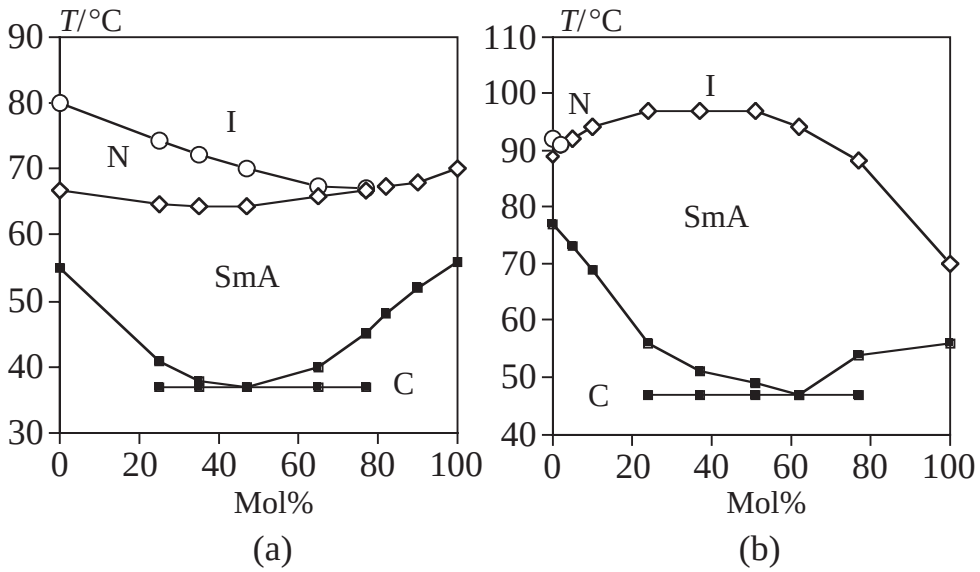

Fig. 5. Binary phase diagrams for the mixtures of: (a) 4-cyano-4′-octyloxybiphenyl (left) and **1**-9 (right), (b) 4-decyloxyphenyl 4-decyloxybenzoate (left) and **1**-9 (right).

6-yl benzoate system. The melting points are summarized in Table 3.

The thermal properties of the LC phases were further examined with binary phase diagrams, and the results are shown in Fig. 5. The SmA phase of 4-cyano-4′-octyloxybiphenyl (8OCB) has been known to exhibit an SmA phase with a partial bilayer arrangement of molecules, namely SmAd.[1] In Fig. 5a, **1**-9 and 8OCB are miscible through the whole range, where both the SmA–N (I) and N–I transition temperatures change continuously and almost linearly, indicating that both components have similar physical properties and mix well not only in the N phase, but also in the SmA one.

On the other hand, for the mixture of **1**-9 and 4-decyloxyphenyl 4-decyloxybenzoate in Fig. 5b, the SmA–N (I) transition temperature shows a notable upward convexity around the center of the diagram. This characteristic feature has been frequently observed in so-called "polar-non-polar" LC mixtures.[10] Therefore, **1**-*n* are considered to posses a polar nature similar to 8OCB.

X-ray Measurement. The layer structures of Sm phases were characterized by a small angle X-ray diffraction measurement.

X-ray profiles for the present compounds consist of two parts in the range between $2\theta = 0$ and 30°. One is a sharp reflection peak observed in the range between $2\theta = 2.5$ and 3.5°, and the other is a broad one between $2\theta = 15$ and 20°. The observed layer spacing d_{obs} of the SmA phase was calculated from the former peak. Although the latter reflection was always observed as a broad peak, the intensity was too small to numerate the position. The d_{obs}s for **1**-*n* are plotted vs temperature in Fig. 6. In Fig. 6a, the d_{obs}s tend to increase a little on reducing temperature. For **1**-11, for example, the reflection peak at 35.2 Å at 76 °C shifts to 35.7 Å at 46 °C. The average d_{obs} of 35.5 Å was plotted against *n* in Fig. 6b and the other d_{obs}s were plotted similarly. As we can see from Fig. 6b, the d_{obs}s have a linear correlation against *n*, where the straight line is expressed by $d_{obs}(\text{Å}) = 1.65n + 17.3$.

The d_{obs}s for **2**-*n* are plotted against temperature and carbon number in Figs. 7a and 7b, respectively. For **2**-5, the recrystallization easily occurred near 120 °C, so that the d_{obs} could be taken only two points at 122 and 125 °C. For **2**-6, an apparent temperature dependency of the d_{obs} was not observed in the range between 112 and 100 °C, while the SmC–SmA (1) transition should occur at 101 °C. Although the X-ray profile of **2**-7 seems to have a broad and weak reflection in the range between $2\theta = 2.5$ and 3.0° around 140 °C, the peak top could not be numerated. The d_{obs}s for the $n = 8$–10 homologues are almost independent of temperature, and the average values are plotted against *n* in Fig. 7b. Apparently, the SmA (2) phase has a different layer structure from the SmA (1) one, i.e., the plots for SmA (2) and SmA (1) phases are expressed by $d_{obs}(\text{Å}) = 1.4n + 24$ and $d_{obs}(\text{Å}) = 1.25n + 18.1$, respectively. It is worthy to note that the constants referring to the LC core length are notably different each other.

In order to correlate these results with molecular parameters, molecular shape and length were estimated by a semi-empirical molecular orbital calculation (MOPAC2000). The most stable conformations of **1**-8 and **2**-6 are shown in Fig. 8. Although a lot of rotational conformers equivalent in point of energy are possible, the conformers illustrated in Figs. 8a and 8b appear to keep the best linearity and might be preferentially present in LC phases as well as the isotropic phase. In the figure, the terminal carbonyl group declines a little from the average long molecular axis and a part of the lactone moiety is off to the side. 2-cyanonaphthalene-6-yl 4-octyloxybenzoate has been reported to experience the phase transition of C·92.8·N·156.1·I (T/°C) type,[11] for comparison the estimated molecular structure is shown in Fig. 8c. As shown in the figure, the core length of **1**-8 is 1.8 Å shorter than that of 2-cyanonaphthalene-6-yl 4-octyloxybenzoate, while the thickness around the LC core portions are quite similar. Surprisingly, the N–I transition temperature of **1**-8 is lower by 94 °C than that of the cyano compound. From these results, it is assumed that the LC properties are influenced not only by the geometrical factor, but

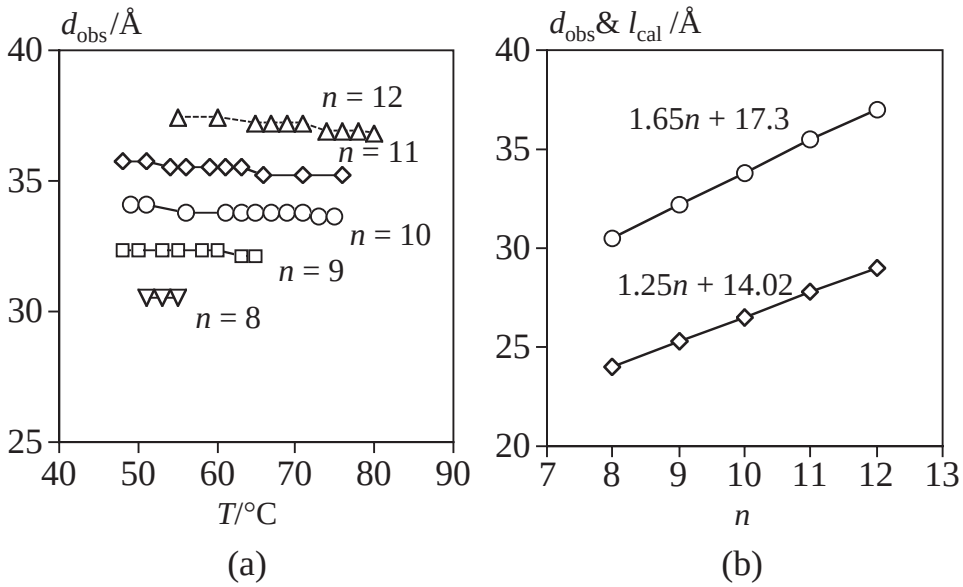

Fig. 6. Plots of: (a) layer spacing (d_{obs}) vs temperature (T), and (b) layer spacing (d_{obs}, ○) and calculated molecular length (l_{cal}, ◇) vs carbon number n for **1**-n.

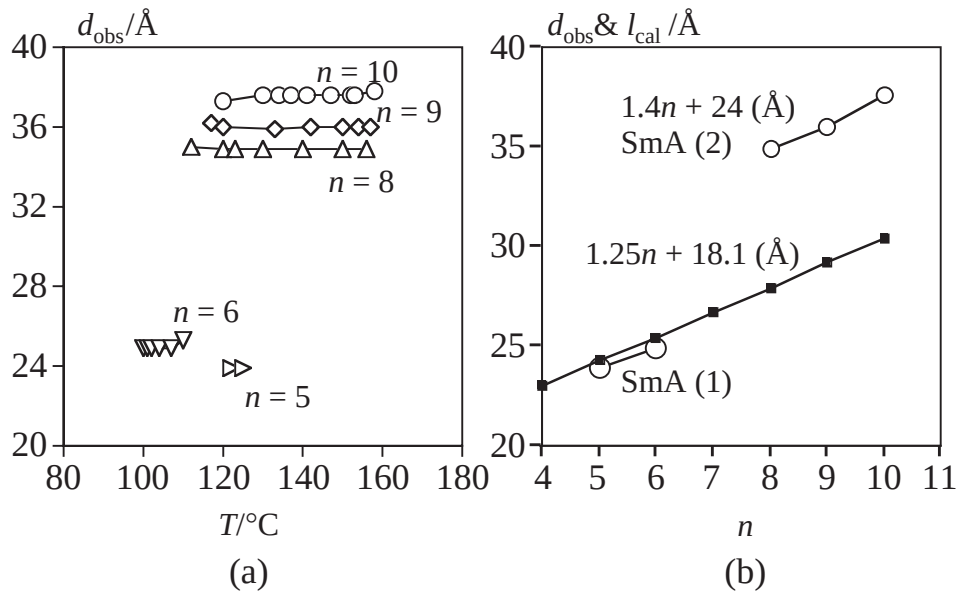

Fig. 7. Plots of: (a) layer spacing (d_{obs}) vs temperature (T), and (b) layer spacing (d_{obs}, ○) and calculated molecular length (l_{cal}, ■) vs carbon number n for **2**-n.

also by the electrostatic one such as magnitude and the direction of the dipole moment arising from the lactone moiety.

The molecular lengths l_{cal} for **1**-n and **2**-n calculated from the conformers are plotted against n in Figs. 6b and 7b, where two straight lines are expressed by l_{cal}(Å) = $1.25n + 14.0$ and $1.25n + 18.1$, respectively. If the hydrocarbon chain extends linearly in the SmA phase and the average rotational axis is arranged orthogonally to the smectic layer, the slope should be $1.25n$ (Å/CH_2), since the C–C bond length and the C–C–C bond angle are 1.51 Å and 111°, respectively, in the saturated hydrocarbon chain, namely an sp^3 hybrid electronic configuration, so that the effective increment is calculated by 1.51 cos(55.5). Therefore, the slopes of 1.25 for both l_{cal} values are a matter of course. The intercepts at $n = 1$ for **1**-n and **2**-n of 15.3 and 19.4, respectively agree with the molecular lengths of the methoxy homologues.

Interestingly, the d_{obs}s for **2**-5 and **2**-6 in Fig. 7b are very close to the l_{cal}s, indicating that the molecules in the SmA (1) phase have a monolayer arrangement, and that the hydrocarbon chain extends linearly and arranges orthogonally to the smectic layer. Based on these results, a possible molecular arrangement in the SmA (1) phase of **2**-6 is proposed and illustrated in Fig. 9a. In Fig. 9a, the terminal hydrocarbon chain extends linearly with keeping rotational and vibrational freedoms, and the average molecular long axis should arrange orthogonally to the smectic layer. For the molecular packing, we assume that the inter-layer dipole–dipole interaction around the lactone moieties stabilizes the monolayer arrangement,

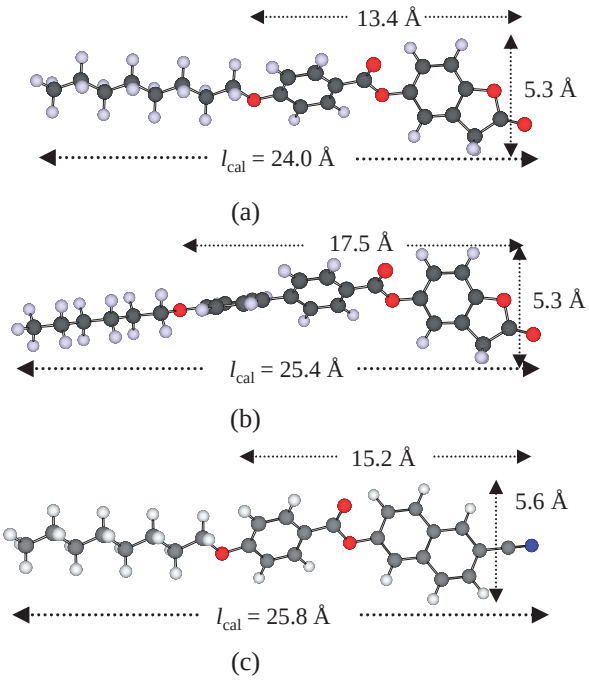

Fig. 8. Molecular structures calculated by MOPAC2000: (a) **1**-8, (b) **2**-6, and (c) 2-cyanonaphthalene-6-yl 4-octyloxybenzoate.

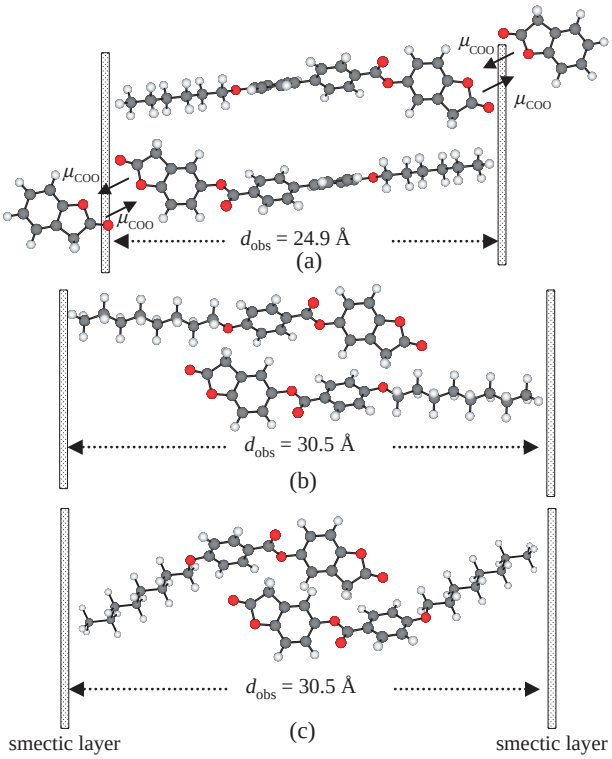

Fig. 9. Possible molecular arrangements of: (a) **2**-6 in SmA (1) phase, (b) **1**-8, and (c) **1**-8 in the SmA (2) phase.

since the carbonyl groups in Fig. 9a arrange side by side. However, the monolayer arrangement seems to become unstable with increasing *n*, since the SmA (1) phase for **2**-*n* is exhibited only by pentyloxy and hexyloxy homologues, simultaneously, the SmA (1)–N transition temperature reduces with increasing *n* and the SmA (1) phase disappears in the heptyloxy and after homologues. As one can assume from Fig. 3b, the SmA (1) phase is exhibited even in the shorter homologues, such as butoxy and propoxy, and the SmA (1)–N transition temperature rises with decreasing *n*. These results indicate that the long hydrocarbon chain at the terminal position is not always necessary for the formation and stabilization of the SmA (1) phase, and some changes in the entire molecular shape due to elongation of the hydrocarbon chain result in decrease of the thermal stability and disappearance of the SmA (1) phase.

As shown in Fig. 3b, the SmC phase below the SmA (1) or N phase is formed by the hexyloxy–octyloxy homologues, where the SmC–SmA (1) or the SmC–N transition temperature reduces with increasing *n*. We assume that for the hexyloxy–octyloxy homologues, the entire molecular shape is bent like Fig. 9c rather than linear in the monolayer SmC phase.

On the other hand, the slope for the SmA phase of **1**-*n* in Fig. 6b is 1.65 and apparently exceeds 1.25. In addition, the d_{obs}s for the SmA phase of **1**-*n* are much larger than the l_{cal}s, where the ratios of d_{obs} to l_{cal} for the octyloxy and dodecyloxy homologues are 1.27 and 1.29, respectively. For this kind of SmA phase, a "partial bilayer" arrangement has been proposed, namely SmAd.[1] The SmAd arrangement is applied to SmA (2) phase of **1**-8, and the possible models are illustrated in Figs. 9b and 9c. Unfortunately, the slope expected from the model in Fig. 9b is in disagreement with the slope of 1.65 obtained from Fig. 6b. If the hydrocarbon chains in the model arrange orthogonally to the SmA layer and the tight dimer structure is kept through the homologues as shown in Fig. 6b, the slope should be 2.50. Therefore, in order to satisfy the results in Fig. 6b, the hydrocarbon chain must tilt to the SmA layer and the entire molecular shape have a bent shape like Fig. 9c, where the tilt angle between the SmA layer and the average rotational axis of the hydrocarbon chain is roughly calculated from the slope in Fig. 6b, giving 45°. The bent shape is assumed to arise from a torsion around the phenyl–O–C (hydrocarbon chain) bond, since the torsional energy is not very high (less than 5 kJ mol^{-1} in our MO calculation). A problem for the arrangement model is that the dipole–dipole interaction assumed in Fig. 9a may not effectively stabilize the dimer structure, since the carbonyl groups within the dimer structure are too far apart, ca. 10 Å in the model, to interact. Therefore, we assume that the bent shape of the molecules due to the long hydrocarbon chain is also an important factor in connection with the most substantial packing in Fig. 9c.

The slope for the SmA (2) phase of **2**-*n* in Fig. 7b is 1.35 and also exceeds 1.25. In addition, the d_{obs}s for the SmA (2) phase are much larger than the l_{cal}, where the ratios of d_{obs} to l_{cal} for the octyloxy and decyloxy homologues are 1.25 and 1.24, respectively.

From these results, the molecular packing in the SmA (2) phase is assumed to be similar to the SmAd type like Fig. 9c, where the tilt angle of the hydrocarbon chain to the smectic layer is roughly calculated from Fig. 7b, giving 57°.

Dielectric Properties. The effect of the lactone group on dielectric properties has been reported in our previous papers.[12,13] Conclusively, the extrapolated dielectric anisotropies $\Delta\varepsilon$s for **1**-4–**1**-6 are 9.2–9.7 in some LC mixtures, suggesting

that the large dipole moment arising from the lactone moiety effectively enhances the positive dielectric anisotropy.

Conclusion

The 3*H*-benzofuran-2-one skeleton is an excellent component of LC materials. The phenyl and biphenyl derivatives facilitate the formation of the SmA phase rather than N phase, where two kinds of SmA phases are formed, namely a fundamental "polar" SmA one with a monolayer arrangement and a "SmAd" one with a partial bilayer phase. Not only polar interactions around the lactone moiety but also the entire molecular shape in connection with the molecular packing are proposed to be important factors for the complex polymesomorphism and diversity of the layer structure in the smectic phases.

Experimental

Materials. Compounds **1**-*n*–**3**-*n* were prepared by conventional esterification (DCC method in THF) with 6-hydroxy-2-oxo-3*H*-benzofuran-2-one and 4-alkoxybenzoic acids, 4-alkoxybiphenyl-4′-carboxylic acids, or 4-alkylbenzoic acids, respectively.

The products were purified by column chromatography on silica gel, where chloroform was preferable as the elution solvent, because the other mixed solvents involving petroleum ether sometimes caused gelation within the column. This tendency was most notable in **2**-*n*. Purity of materials was checked by ^{1}H NMR and HPLC.

Method. The transition temperatures and latent heats were determined using a Seiko SSC-5200 DSC, where indium (99.9%) was used as the calibration standard (mp 156.6 °C, 28.4 J g^{-1}). Normally, the DSC thermogram was operated at a heating or a cooling rate of 5 °C min^{-1}.

The mesophases were characterized using a Nikon POH polarizing microscope fitted with a Mettler thermo-control system (FP-900).

X-ray diffraction experiments for the SmA phases were performed using a Rigaku-denki RINT 2200 diffractometer, where Cu Kα ($l = 1.541$ Å) was used as the X-ray source. The reflection angle was calibrated by comparing both right and left angles. The temperature was controlled using a Rigaku PTC-20A controller. The samples filled into a quartz capillary (1.5 mmϕ) were oriented by a constant magnetic field (480 G). The samples were heated to the isotropic temperature and measurements were carried out during the cooling process.

Molecular parameters were estimated by a semi-empirical molecular orbital calculation (MOPAC2000), where the heat of formation was minimized by the AM1 method.

References

1 G. W. Gray, H. W. Goodby, *Smectic Liquid Crystals*, Heyden & Son Inc., Philadelphia, **1984**, p. 134.
2 E. C. Hurdis, *J. Am. Chem. Soc.* **1943**, *65*, 89.
3 Y. Masuda, Y. Sakurai, H. Sugiura, S. Miyake, S. Takenaka, S. Kusabayashi, *Liq. Cryst.* **1991**, *10*, 623.
4 H. E. Watson, G. P. Kane, K. L. Ramaswamy, *Proc. R. Soc. London, Ser. A* **1936**, *156*, 137.
5 M. Puchalik, *Acta Phys. Pol.* **1950**, *10*, 89.
6 Y. S. Li, *J. Mol. Struct.* **1987**, *159*, 37.
7 L. G. Gloves, S. Sugden, *J. Chem. Soc.* **1934**, 1094.
8 J. W. Goodby, T. M. Leslie, P. E. Cladis, P. L. Finn, *Liq. Cryst. Ordered Fluids* **1984**, *4*, 89.
9 A. Boller, H. Scherrer, M. Schadt, P. Wild, *Proc. IEEE* **1972**, *60*, 1002.
10 H. Kelker, R. Hatz, *Handbook of Liquid Crystals*, Verlag Chemie, Weinheim, **1980**, p. 340.
11 D. Coates, G. W. Gray, *Mol. Cryst. Liq. Cryst.* **1976**, *37*, 249.
12 Y. Morita, T. Tasaka, K. Kabu, H. Okamoto, S. Takenaka, *IDW '03*, **2003**, p. 217.
13 Y. Morita, T. Tasaka, R. Yamaguchi, H. Okamoto, S. Takenaka, *Abstract of ILCC2004*, **2004**, p. 968.